Poisoning effects of sulfur dioxide in an air stream on spatial proton exchange membrane fuel cell performance

Tatyana Reshetenko [a],[*], Vincent Laue [b], Ulrike Krewer [b], Katerina Artyushkova [c]

[a] *Hawaii Natural Energy Institute, University of Hawaii, Honolulu, HI, 96822, USA*
[b] *Institute of Energy and Process Systems Engineering, Technische Universitaet Braunschweig, Franz-Liszt-Straße 35, 38106, Braunschweig, Germany*
[c] *Center for Micro-Engineered Materials, University of New Mexico, Albuquerque, NM, 87106, USA*

HIGHLIGHTS

- Effects of sulfur dioxide in air on PEMFC were studied with a segmented cell.
- 2 ppm SO_2 caused voltage loss of 60 and 295 mV at 0.2 and 1.0 A cm^{-2}, respectively.
- SO_2 is oxidized at potentials corresponding to 0.2 A cm^{-2}
- SO_2 reduction to zero-valent sulfur takes place at 1.0 A cm^{-2} conditions.
- Physics-based mathematical model was developed for analysis of SO_2 effects on PEMFC.

ARTICLE INFO

ABSTRACT

The paper examines spatial and temporal proton exchange membrane fuel cell (PEMFC) performance under exposure to SO_2 in an air stream at low and high operating currents. Cathode poisoning by 2 ppm SO_2 resulted in cell voltage losses of 60 and 295 mV for overall cell currents of 0.2 and 1.0 A cm^{-2}, respectively. The voltage drop was accompanied by localized current redistributions, which depend on the operating current hold. The observed spatial PEMFC behavior is attributed to different electrochemical reactions of adsorbed SO_2 occurring at high and low cathode potentials. SO_2 is mainly oxidized at potentials corresponding to 0.2 A cm^{-2}, while reduction to zero-valent sulfur takes place at 1.0 A cm^{-2}, as confirmed by XPS. Full self-recovery was not observed for either operating current hold, and only potential cycling recovered the performances. Moreover, comparison of the initial and after-poisoning electrochemical PEMFC parameters revealed that SO_2 exposure led to a decrease in Pt electrochemical surface area due to growth of the Pt particle size and caused final performance losses of 20–30 and 25–50 mV for low and high current operations. A physics-based mathematical model was successfully developed and applied for analysis of SO_2 effects on PEMFC performance.

1. Introduction

The proton exchange membrane fuel cell (PEMFC) is an alternative clean energy technology that directly converts chemical energy to electricity and has become highly attractive as a power source for automotive, portable and stationary applications. Reliable, stable and durable fuel cell performance under various operating and environmental conditions is required to overcome the early stage of technology commercialization. Generation of electricity by fuel cells relies on continuous supply of fuel (hydrogen) at the anode and oxidant (air) at the cathode electrodes, and the PEMFC efficiency strongly depends on the purity of both reagents. The purity of hydrogen fuel is controlled during its production via electrolysis or the reforming process of natural gas, whereas ambient air is typically used as an oxidant. Atmospheric air usually contains a variety of inorganics, volatile organic compounds (VOCs) and particulates originating from natural and/or anthropogenic sources of emission, leading to PEMFC performance decline and degradation [1–6].

Our previous work systematically studied PEMFC behavior under exposure to different organic airborne contaminants [7–11]. The selected VOCs represent different classes of organic compounds as model contaminants which are widely used in the chemical industry and in household goods, and their concentrations in air depend on urban or

rural locations, varying in the range of 0.1–100 ppb [12–15]. It was shown that organic pollutants negatively affected PEMFC operation, but for a majority of cases, performance was restored immediately when introduction of the contaminants into the air stream was stopped [5, 7–10,16,17], and only certain warfare agents, alkyl halides, and halides caused irreversible deterioration of fuel cells [1,11,18]. Evaluation of PEMFC performance under exposure to the main inorganic airborne contaminants revealed that NH_3 and NO_x caused moderate and reversible performance loss [1,3,19–29], while sulfur-containing compounds (SO_2, H_2S and COS) resulted in the most drastic and non-recoverable impacts on cathode electrodes [1,3,19–23,26,27,30–40].

Out of all studied air pollutants, SO_2 has particular importance for detailed evaluation due to its various sources of emissions, wide range of concentrations and its detrimental impact on PEMFC performance. The most important sources of SO_2 are anthropogenic and include fossil fuel combustion (vehicle and industrial exhaust, coal and oil-fed power plants), manufacturing of sulfuric acid, conversion of wood pulp to paper and production of elemental sulfur. Moreover, naturally occurring processes such as volcanic eruption act as significant sources for SO_2 emission and should be considered for fuel cell applications at close proximity to active volcanos. Annual average SO_2 concentrations are in the range of 5–20 ppb (15–20 µg m^{-3}) in most world cities, but at roadsides and industrial areas, the SO_2 concentration can reach higher levels (400–750 ppb) [41,42], and volcanic eruption can increase the SO_2 level up to several ppm [43–45].

Analysis of published research papers demonstrated that the effects of SO_2 were studied using PEMFCs operating under constant current [1, 19,20,27,36] or voltage hold conditions [3,21,22,30–32,34,40]. Variations in operating conditions render comparison of the experimental data challenging, but we could conclude that several ppm of SO_2 caused a significant PEMFC performance drop in the range of 200–300 mV in high power operation, and full recovery to the initial performance did not occur when SO_2 injection in the air stream was stopped. For example, the fuel cell voltage loss under exposure to 2 ppm SO_2 at a constant current hold of 1.0 A cm^{-2} and 80 °C was in the range of 200–250 mV [19,40]. At the same time, D. Imamura reported a voltage drop of ~300 mV for a fuel cell operated at similar conditions but with an SO_2 concentration of 1 ppm [20]. The difference in these results might be attributed to different suppliers of the membrane electrode

assemblies (MEAs). It should be noted that prior research was primarily performed using a single cell [3,19–23,27,30–37,40] or stack [6,26,38], and both approaches provided only average values of current and voltage for an MEA active area. In contrast, a segmented cell system reveals locally resolved electrochemical parameters such as voltage, current and impedance and is a powerful tool for gaining detailed information on fuel cell performance under various operating conditions, i.e., exposure to different fuel or air impurities [7–11,46].

In addition, a computational approach that investigates the effects of air impurities on PEMFC performance offers several important advantages. Using phenomenological models allows us to identify the reaction mechanisms and kinetics that properly correlates with the existing fuel cell performance and assess the effects of additional, previously unexplored contaminants. The simulation results also might quantify fuel and air purity standards and assist in design of new fuel cell components. Finally, a modeling approach could aid in obtaining details with respect to long-term contaminant effects on PEMFCs at extremely low levels (~1 ppb). Although these concentrations are large enough to affect the kinetics of the fuel cell reactions, they are difficult to precisely detect and control in an experimental setting. Therefore, a well-designed computational approach might more accurately evaluate the durability and sustainability of PEMFCs.

A transient kinetic model describing anode H_2S PEMFC contamination was developed by Z. Shi et al. [47]. The authors assumed electrochemical dissociation of H_2S with formation of adsorbed sulfur on Pt, and the sulfur surface coverage was determined as a function of relevant chemical reaction rates, concentrations of H_2S and H_2, anode overpotential and test duration. Later, Z. Shi and coauthors proposed a general model for air-side feed stream contamination that was capable of simulating both transient and steady state performance of PEMFC in the presence of airborne contaminants [48]. The model considered the oxygen reduction reaction (ORR) mechanism, contaminant surface adsorption/desorption and electrochemical reaction kinetics. However, it did not include the self-recovery process of PEMFCs. The generic kinetic loss model was introduced by J. St-Pierre and offered a single exponential function for the current response to poisoning in constant voltage cell operation and a further single exponential function for the current response at the recovery stage [49]. While emerging PEMFCs models are based on extensive and descriptive systems of equations, these simulations typically rely on a very large number of parameters, which sometimes do not have well-defined physical meanings. These variables might have limited practical value because certain parameters of intermolecular interactions and rate constants are difficult to measure or control in PEMFCs. Models with fewer parameters, as well as models that define the parameters based on controllable experimental conditions, are expected to reveal additional insights into the effects of air contaminants.

The current work is a continuation of our previously published results and presents detailed studies of localized high-Pt loaded PEMFC performance under cathode exposure to SO_2. Moreover, a physics-based mathematical model for SO_2 poisoning of PEMFC was developed to reveal a feasible mechanism, explain the experimental findings and gain physical insights into the poisoning process.

2. Modeling of SO_2 contamination. Model setup and governing equations

The model domain contains *N* serially connected flow compartments for the cathode, and each of them including the gas diffusion layer (GDL) is suggested to have no gradient, i.e. be ideally mixed. The model setup is related to the segmented PEMFC also applied in the experiments. The ionomer phase covering the Pt catalyst is discretized, and diffusion by Fick's law is assumed for O_2 and SO_2:

$$\frac{\partial c}{\partial t}   D \frac{\partial^2 c}{\partial x^2} \tag{1}$$

The mass transport coefficients of oxygen can be taken directly from the experimental results of Reshetenko et al. measured on the same system [50]. The SO_2 reactions take place at the interface between the ionomer phase and Pt. For all electrochemical reactions, Butler-Volmer kinetics are applied:

$$r = k_f \prod_i^{educts} \frac{c_i}{c_{i,0}} \cdot \exp\left(\alpha \frac{F}{RT}\eta\right) - k_b \prod_i^{products} \frac{c_i}{c_{i,0}} \cdot \exp\left(-(1-\alpha)\frac{F}{RT}\eta\right) \quad (2)$$

wherein the overpotential is

$$\eta = \Delta E - E_0 \quad (3)$$

To ensure equal potentials in all segments, the current distribution between segments is derived from Ohm's and Kirchhoff's laws:

$$E_{cell} = \Delta E_i - I_i \cdot R_i, \quad \forall i \in \{1, ..., N\} \quad (4)$$

$$I_{cell} = \sum_{i=1}^{N} I_i \quad (5)$$

The resistance R_i is derived from the conducted electrochemical impedance spectroscopy (EIS) experiments and is related to the bipolar plates etc. The current I_i is the current in one segment of the segmented bipolar plate. All bipolar plates are supposed to be in an ideal parallel connection. The current is the input to the charge balance

$$\frac{d\eta_j}{dt} = \frac{1}{C_{DL}}\left(I_j - F\sum_i z_i r_{i,j}\right), \quad \forall i \in \{1, ..., N\} \quad (6)$$

controlling the potential at the Pt-to-ionomer interface. For all adsorbed species j, the surface concentration $\theta_{i,j}$ is determined

$$\frac{d\theta_{i,j}}{dt} = \sum_l r_{i,l} \cdot \nu_{l,j} \quad (7)$$

wherein index i denotes the different segments, l is the reaction, j is the species, and $\nu_{l,j}$ is the stoichiometric coefficient of species j in reaction l. For clarity, a normalized surface coverage $\Theta_{i,j}$ is introduced. The surface coverage of the free surface sites is defined as

$$\Theta_{free} = 1 - \sum_j \Theta_{i,j} \quad \forall i \in \{1, ..., N\}, \quad (8)$$

wherein the index j denotes the different adsorbed species. In summary, the spatially discretized state variables in the flow field and ionomer phase are O_2 and SO_2, and the state variables as adsorbed species are SO_2, SO, S, SO_3^{2-}, O_2, and H_2O. The evaluated reaction kinetic schemes are explained in detail in section 4.5. The purpose of this model is not primarily to investigate spatial charge or mass transport in the fuel cell, but provide a framework for study of different reaction mechanisms and reveal the least complex mechanism that is feasible to explain the experimental findings. It should be noted that the proposed model is also able to simulate non-constant current profiles. In this work, we focus on constant current to match the experiments.

3. Experimental

All experimental tests were conducted using a fuel cell test station that was modified in-house to the required specifications, a segmented cell system developed at the Hawaii Natural Energy Institute and a Solartron SI 1287/electrochemical interface. The segmented cell setup consists of the cell hardware, the custom-designed current transducer system, the data acquisition device and a single cell test station. The HNEI system has closed-loop Hall sensors (Honeywell CSNN 191) for current detection and a data acquisition system, which allows simultaneous data collection from 10 current channels. The segmented cell system is typically operated as a single cell using the test station and standard testing protocols, which simulates conditions that are identical

to the real case because only the total cell current is controlled. Details of the segmented cell system can be found in our previous publications [51, 52].

For this work, we used commercially available 100 cm^2 MEA supplied by Gore. The anode and cathode were made of Pt/C catalysts with a loading of 0.4 mg$_{Pt}$ cm^{-2}. Sigracet 25 BCE was applied as the anode and cathode GDLs. The cathode used a segmented GDL and gasket configuration, a single GDL was applied at the anode, and the total active area of the MEA was 76 cm^2 due to the segmentation. The gasket material was made of Teflon, with thicknesses of 125 μm for the anode and the cathode. The break-in procedure included 20 voltage cycles from 0.85 V (5 min) to 0.6 V (10 min) and constant voltage hold at 0.6 V for 2 h. The operating conditions were 100% RH, 150 kPa backpressure and stoichiometry of 2 for both electrodes, the cell temperature was 80 °C.

The anode/cathode testing conditions for the contamination experiments were H_2/air, 2/2 stoichiometry, 100/50% relative humidity and 150/150 kPa backpressure. The cell temperature was 80 °C. The MEA was operated under galvanostatic control of the whole cell current. The SO_2 concentration was 2 ppm in the air stream. The polarization curves (VI curves) in the H_2/air gas configuration were measured under the same conditions as in the contamination experiment. The VI curves were also recorded in the H_2/He + O_2 (21 vol%) and H_2/O_2 gas configurations to determine the activation, ohmic and mass transfer overpotentials, as previously described in Ref. [51].

EIS measurements were performed to determine the high-frequency resistances (HFR) and to record the impedance spectra for all ten segments as well as the overall cell. The frequency range was 0.05 Hz–10000 Hz, and the amplitude of the current perturbation signal was 2 A, which caused a cell voltage amplitude of 10 mV or lower.

To obtain the electrochemical surface area (ECA), cyclic voltammetry (CV) experiments were performed using a Solartron SI 1287/electrochemical interface. The CV was conducted at a cell temperature of 35 °C with a scan rate of 20 mV s^{-1} while 100% humidified hydrogen and nitrogen were supplied to the reference/counter and working electrodes, respectively, at a flow rate of 0.750 l min^{-1}. For each measurement, 3 cycles were applied over a potential range from 0.015–1.1 V vs. the hydrogen reversible electrode. The hydrogen desorption peak area of the third cycle was used to determine the ECA. To recover the cathode performance after SO_2 poisoning, 13 scans were performed from 0.01–1.1 V with 3 addition scans with extended upper potentials to 1.4 V.

MEAs, anode and cathode catalysts were studied by scanning electron microscopy (SEM), transmission electron microscopy (TEM) and X-ray photoelectron spectroscopy (XPS). A Kratos XPS ultra DLD spectrometer operating with a Al Kα monochromatic source at 225 W was used to obtain high-resolution F 1s, C 1s, O 1s, Pt 4f and S 2p spectra. SEM images of the MEAs were obtained with a Hitachi S-4800 field emission microscope with an accelerating voltage of 5 kV. TEM studies of the catalysts were performed using a Hitachi HT-7700 instrument.

4. Results and discussion

4.1. Effects of SO$_2$ on spatial PEMFC performance at low and high current densities

Profiles of the segment voltages and current densities normalized to their initial values under 2 ppm SO_2 poisoning at overall cell currents of 0.2 and 1.0 A cm^{-2} are shown at Fig. 1. The cell was operated with pure air for the first 16 h to acquire the initial performance at low and high constant current holds. The average cell voltages of 0.790 and 0.665 V were reached in the pre-poisoning period of the tests for 0.2 and 1.0 A cm^{-2}, respectively. The initial distribution of the current density ranged from 0.19 to 0.24 A cm^{-2} at 0.2 A cm^{-2} of the total current of the whole cell, and the current hold at 1.0 A cm^{-2} resulted in local current inhomogeneity from 0.94 to 1.05 A cm^{-2}. Introduction of 2 ppm SO_2
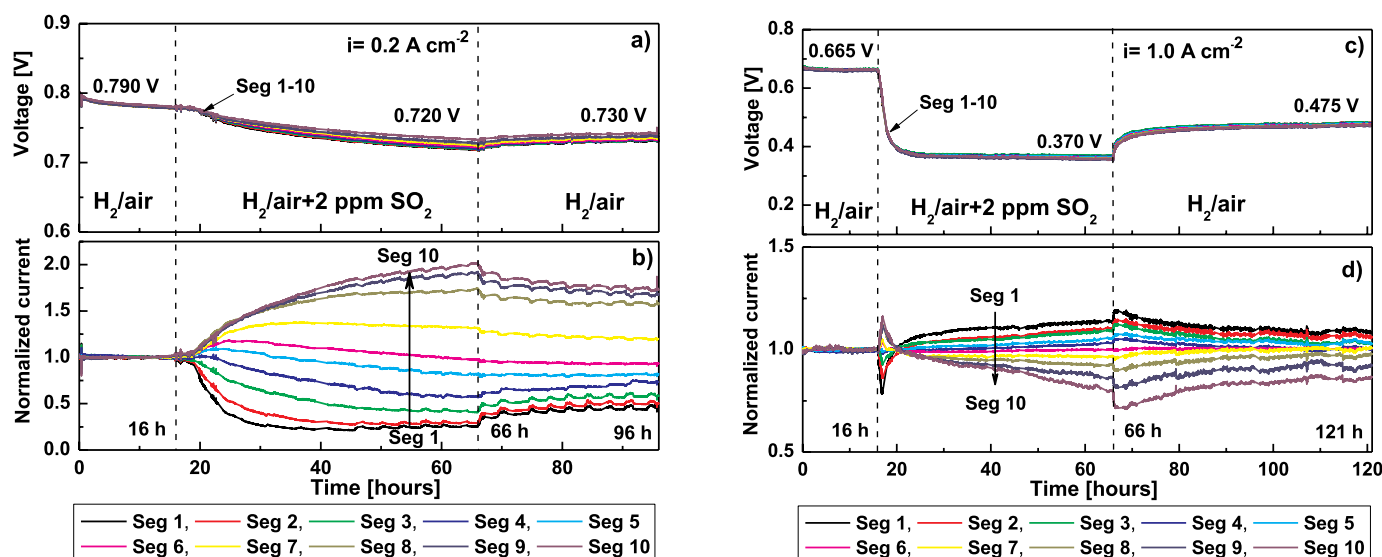
Fig. 1. Voltage and normalized current densities of PEMFC segments under cathode poisoning of 2 ppm SO_2 for total cell current densities of 0.2 (a, b) and 1.0 A cm^{-2} (c, d). Anode/cathode: H_2/air, 2/2 stoichiometry, 100/50% RH, 150/150 kPa, 80 °C.

into the air stream caused a decrease in the cell and individual segment voltages. The performance drops at steady state were 70 and 295 mV for low and high current operation modes, respectively (Fig. 1a, c), which correlate well with previously published results [19–23,30,40]. It should be noted that changes in the cell response were detected after 3–5 h of PEMFC poisoning at 0.2 A cm^{-2}, but such a transition period was not observed at 1.0 A cm^{-2} conditions. The delay in response at low current operation could be attributed to adsorption of SO_x species on Pt surface without electrochemical reactions until SO_x coverage reached a certain critical value when it affected the cell voltage. The performance loss at both constant current holds was entailed by a significant local current redistribution, which depended on the operating conditions.

At low current, SO_2 cathode poisoning caused a decrease in the spatial performances of the inlet segments 1–4, and the outlet segments 8–10 generated higher current compared with the initial values. The current density distribution ranged from 75% for segments 1 and 2 to +95–100% for segments 9 and 10 (Fig. 1b). We presumed that adsorption of SO_2 and its chemical/electrochemical reactions occurred mainly at the inlet portion of the MEA and resulted in a decrease in the local current density. The remainder of the electrode area appeared to be unpoisoned and had to produce higher current to ensure an overall 0.2 A cm^{-2} because the cell was operated under galvanostatic control of load. A similar current distribution pattern was found for CO anode poisoning, acetylene and benzene contamination of cathode at low current conditions [7,9,46].

A complex behavior in the spatial performance was detected with SO_2 exposure at high current (Fig. 1d). At the beginning of the contamination, the current densities of inlet segments 1-5 decreased while the performance of the outlet segments 6–10 increased. As soon as the local currents reached their extremum values, within 1 h of SO_2 injection, a reversal of the spatial performance occurred in which the inlet portion of MEA produced higher current than the outlet segments. The extremum values of the segment current corresponded to an inflection point of the voltage profiles at 0.520–0.540 V. At steady state, the current density distribution varied from 20% for segment 10 to +14% for segment 1. Similar behavior was previously observed with CH_3CN exposure of PEMFC [8]. The obtained spatial performance in high current operation is likely affected by electrochemical SO_2 transformation at the Pt cathode, which will be discussed later in this paper.

The cell and segments did not fully restore their performance (voltage and local currents) after stopping of SO_2 exposure during low and high current densities (Fig. 1b, d). At the self-recovery stage, the cell

voltage reached 0.730 V (vs. the initial 0.790 V) and 0.475 V (vs. the initial 0.665 V) at 0.2 and 1.0 A cm^{-2}.

Spatial impedance spectra for the overall cell and selected segments under SO_2 exposure are presented in Fig. 2. The initial EIS curves were recorded in pure air after 15 h of operation for low and high current densities. The spectra consisted of a high-frequency cathode arc attributed to charge transfer resistance and double layer capacitance for the oxygen reduction reaction and a low-frequency loop representing the mass transport limitation at the cathode. An increase in the low-frequency arc occurred with current and from the inlet to the outlet location due to oxygen consumption and water accumulation downstream.

The EIS effects of SO_2 introduction into the air stream at 0.2 A cm^{-2} were detected only after 5 h of exposure, which is in agreement with the spatial fuel cell performance (Fig. 2a, pathway 1). The impurity caused an initial increase in the impedance response for inlet segments 1–3, but segments 4–6 did not show any changes. Moreover, segments 7–10 revealed a slight decrease in impedance. Further SO_2 injection continued this trend, i.e., the inlet of MEA demonstrated a growth in charge and mass transfer resistances, whereas the outlet part clearly showed a decline in impedance (Fig. 2a, pathways 2 and 3). Steady state was reached after 40 h of cell contamination. The cell self-recovery resulted in a decrease in the impedance response for the inlet segments and an increase for the outlet (Fig. 2a, pathways 4 and 5). Despite 30 h of operation in pure air, the segments did not exhibit restoration of their initial impedance.

Fuel cell exposure to SO_2 at 1.0 A cm^{-2} revealed a different behavior. The charge and mass transfer resistances of all segments increased significantly after 1 h of SO_2 exposure (Fig. 2b, pathway 1). At the same time, a low-frequency pseudo-inductive behavior was observed for all segments. Interestingly, this observation corresponds to the inflection point of the voltage profile (0.520–0.540 V) and the extremum values of the segment current densities. A low-frequency inductance in the impedance spectra indicates successive electron transfer reactions involving adsorbed contaminant species and proceeding with the formation of intermediates on the Pt surface [53–57]. Moreover, such inductance means that the current signal follows a perturbation with a phase delay due to the slow relaxation of adsorbate coverage compared with the oxygen reduction. Previously, the low-frequency inductive loop was detected for PEMFCs exposed to C_2H_2, CH_3CN, CH_3Br and naphthalene at potentials at which electroreduction of contaminants can take place in parallel with oxygen reduction [7–9,11]. Low frequency
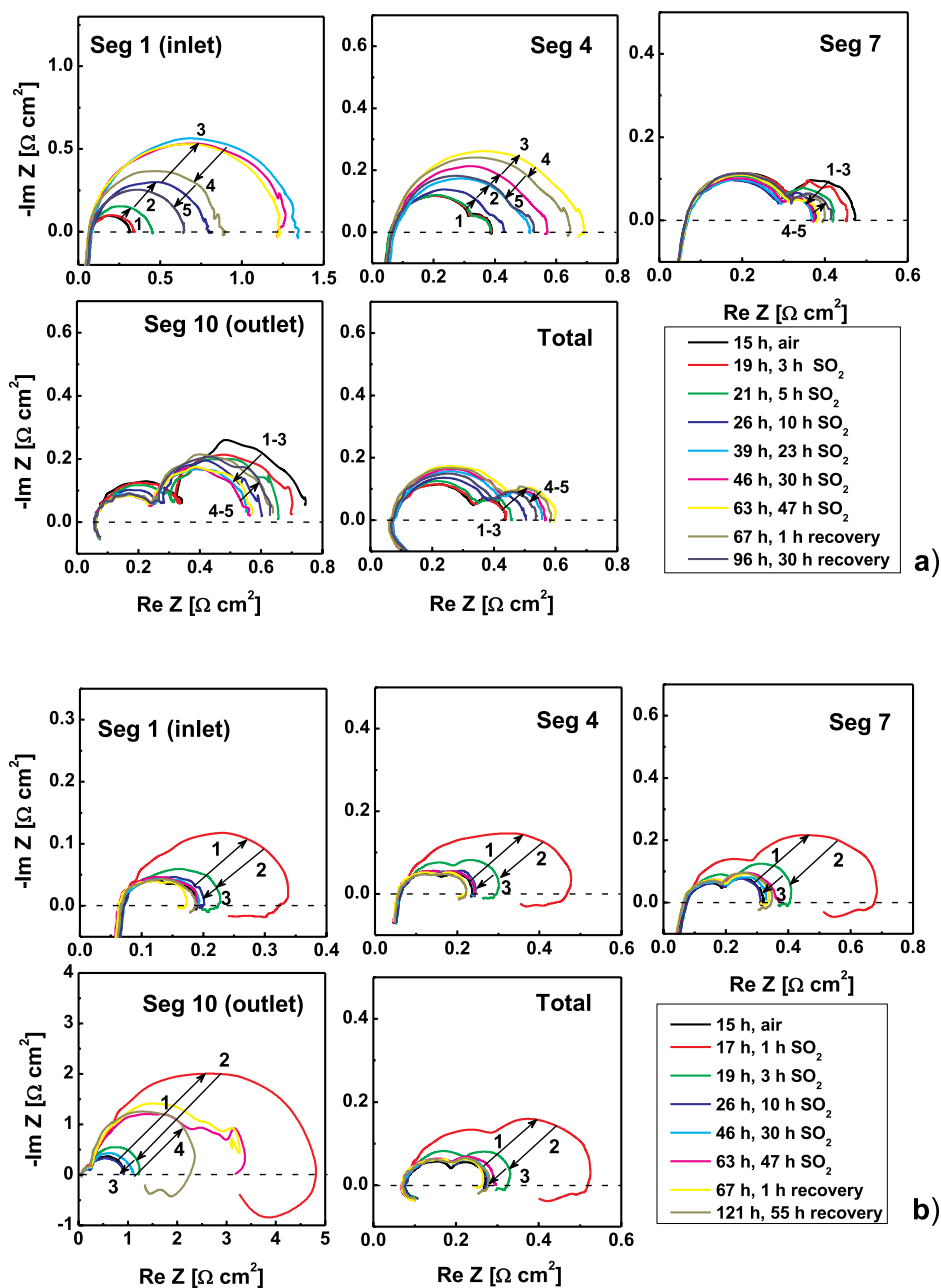
Fig. 2. EIS for segments 1, 4, 7, 10 and the total cell under 2 ppm SO_2 exposure at overall current density of 0.2 (a) and 1.0 A cm^{-2} (b). Anode/cathode: H_2/air, 2/2 stoichiometry, 100/50% RH, 150/150 kPa, 80 °C.

inductive behavior was also observed in direct methanol fuel cells, and kinetic models could reproduce the behavior using a methanol oxidation mechanism with adsorbed species and sequential steps of similar velocity [58]. The low-frequency inductance in the SO_2 case allows us to believe that electroreduction of sulfur-containing species can occur at these operating conditions. Further, SO_2 exposure decreased the impedance of the segments, except for segments 9 and 10, which displayed complicated EIS behavior at low frequency range (Fig. 2b, pathway 2 for segments 1, 4, 7 and the total cell; pathway 3 for segment 10). The EIS response of the outlet segments was most likely due to water accumulation and flooding, which led to an increase in impedance and appearance noticeable noise patterns. Operation with pure air after poisoning resulted in partial local recovery (Fig. 2b, pathway 3 for segments 1, 4, 7 and the total cell; pathway 4 for segment 10).

4.2. Analysis of ECA and PEMFC performance before and after SO_2 exposure

To understand the effects of SO_2 on PEMFCs, the diagnostic results at the beginning of the test (BOT) and the end of the contamination test (EOT) were compared. The BOT and EOT consisted of CV and VI with EIS using different gas configurations to measure the performance and voltage losses [51].

Fig. 3a and b presents the sequence of several CV cycles of a Pt cathode contaminated by SO_2 at 0.2 and 1.0 A cm^{-2}. The graphs also show a BOT scan for both cases as a reference. During the first positive sweep from 0.1 to 1.15 V, the anodic current in the hydrogen region (0.1–0.3 V) is lower for the poisoned cathodes compared with the following scans and BOT curves, which is more pronounced for the cell exposed to SO_2 at high current (Fig. 3a and b). In addition, a broad anodic peak is present at 1.1–1.2 V due to electrochemical oxidation of
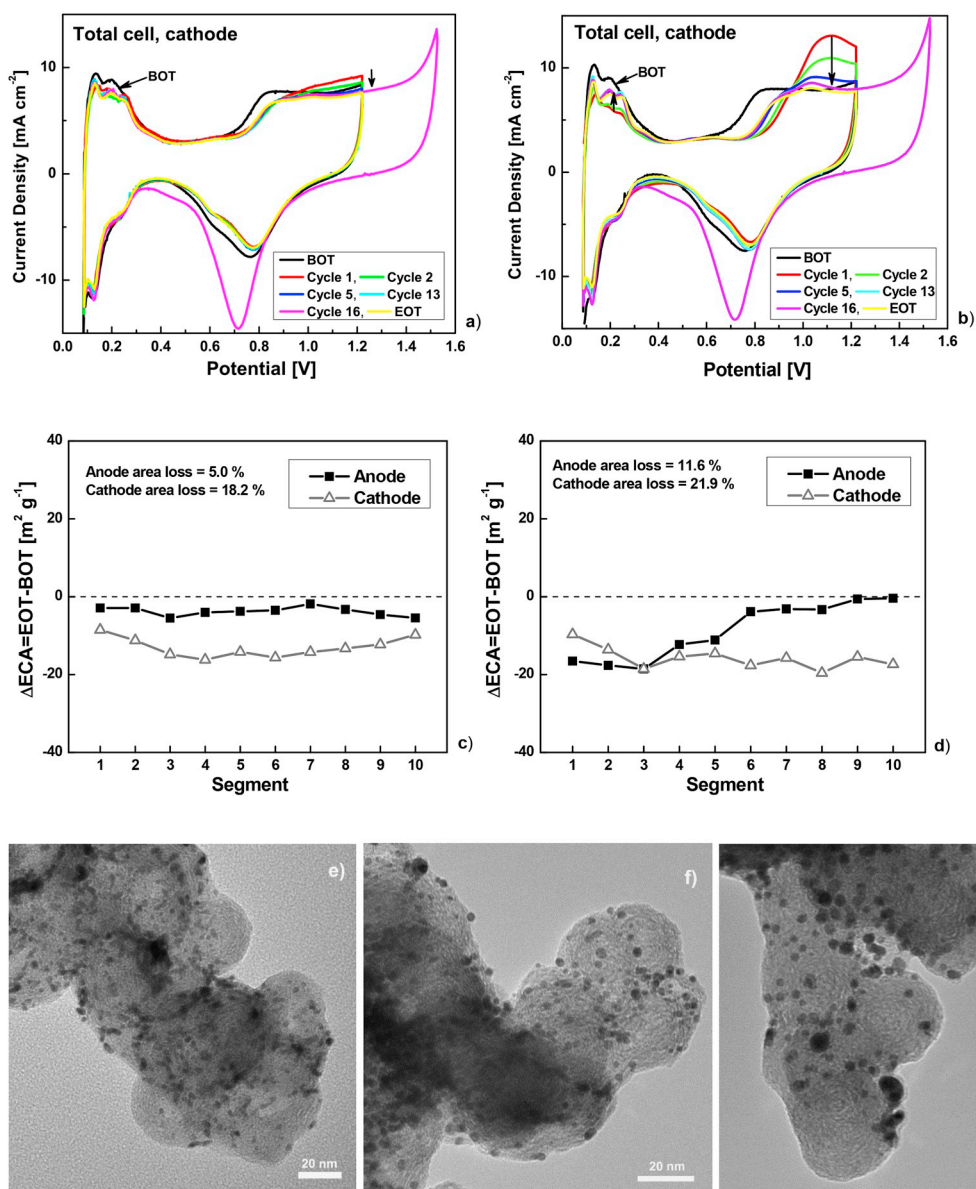
Fig. 3. Cathode CV curves measured for the whole cell after 2 ppm SO_2 exposure at 0.2 (a) and 1.0 A cm^{-2} (b). Distributions of anode and cathode ECA differences between values after (EOT) and before (BOT) SO_2 poisoning at 0.2 (c) and 1.0 A cm^{-2} (d) tests. Anode/cathode: H_2/N_2, 0.75/0.75 l min^{-1}, 100/100% RH, 35 °C, ambient pressure, 20 mV s^{-1}. TEM images of fresh cathode Pt/C catalyst (e), after reference test at constant current hold of 1.0 A cm^{-2} (f) and exposed to SO_2 at 1.0 A cm^{-2} (g).

zero-valent sulfur (S^0) species to SO_4^{2-} [59–61]. This peak is less pronounced for the cell operated at low current, implying that the amount of sulfur-containing species on the Pt surface is less than that at 1.0 A cm^{-2} (Fig. 3a and b). However, despite electrochemical removal of residual sulfur-containing species from the cathode, a loss of Pt ECA occurs for both conditions. Moreover, a shift in the potential for the Pt oxide formation from 0.67 to 0.76 V and a small peak at 1.05 V remain, indicating irreversible changes in the catalyst or the presence of some sulfur species. After the first 13 scans from 0.1 to 1.15 V, additionally three CV cycles were performed with upper potential limit to 1.5 V. A comparison of these two sets of CV scans showed that cycling to 1.5 V did not additionally oxidize any zero-valent sulfur species on the Pt surface and did not increase ECA. It should also be noted that CV cycling was performed after H_2/N_2 and N_2/N_2 purges of the cell anode/cathode, respectively. These operations decreased the cell potential to 0.1 V or lower, which is favorable for reduction of sulfur-oxygen species to S^0 [31,59–63]. Subsequently, this zero-valent sulfur was detected and

removed in CV scans at potentials greater than 1.0 V. The obtained CV results are in agreement with those reported in the literature [30,31,40, 59,60,64–66].

Distributions of the anode and cathode ECAs differences between EOT and BOT are shown at Fig. 3b and c. The decrease in anode and cathode ECAs after the SO_2 contamination test at low current was quite uniform across the MEA active area, but a different behavior was observed at high current conditions. The anode ECA has a higher loss at the inlet part of the MEA (segments 1–5), whereas the outlet segments show less surface area decrease. The cathode ECA loss was found to increase downstream, which can be associated with water accumulation and non-uniform conditions at high current density operation.

For comparison purposes, a reference test was performed at a constant current hold of 1.0 A cm^{-2} for 120 h at the same operating conditions as the poisoning tests. The cell voltage during the constant current hold was 0.680 V and did not show any performance loss. The summary results in Table 1 clearly show that SO_2 and its derivatives negatively

Table 1
Electrochemical surface area of the samples before and after contamination tests.

Operating conditions	Anode ECA [$m^2 g^{-1}$]		Cathode ECA [$m^2 g^{-1}$]		ΔECA [%]	
	BOT	EOT	BOT	EOT	anode	cathode
2 ppm SO_2, 0.2 A cm^{-2}	75.2	71.4	69.2	56.2	5.0	18.2
2 ppm SO_2, 1.0 A cm^{-2}	75.1	66.4	72.1	56.3	11.6	21.9
Reference, 1.0 A cm^{-2}	70.5	67.4	65.6	57.7	4.4	12.0

affected the cathode ECA and caused a significant loss of 21.9% compared with 12% for the reference test. The electrochemical data are strongly confirmed by TEM evaluation of the catalysts (Fig. 3e–g). The Pt particle sizes from the anode and cathode in fresh MEA were in the range of 2.0–2.5 nm (Fig. 3e). Operation in pure air resulted in an increase in the cathode Pt/C particle diameter to 3–5 nm (Fig. 3f), while SO_2 cathode exposure caused an additional growth in the Pt particle size with a broad distribution from 3 to 10 nm (Fig. 3g). This observation allowed us to conclude that SO_2 and its derivatives contribute to the increase in Pt particle size and ECA loss. The anode catalyst from the reference test demonstrated only a slight increase in the particle size, whereas operation with SO_2 at high current density led to a pronounced increase in the Pt diameter to 3–5 nm.

Fig. 4 compares the spatial polarization curves before and after SO_2 contamination tests at 0.2 and 1.0 A cm^{-2}. The VIs were measured after CV scans. Performance loss was observed even after the recovery CV procedure, and the voltage drop was found to be 20–30 and 25–50 mV for low and high current holds, respectively. A comparison of the BOT and EOT performances for the reference test did not reveal any voltage loss greater than 5 mV. Thus, the observed irreversible degradation of the MEAs exposed to SO_2 is caused by the negative effect of the impurity. Interestingly, exposure to SO_2 at low current hold resulted in less PEMFC degradation than operation at high current (20–30 mV vs. 20–65 mV). To understand the origin of the voltage losses, the BOT and EOT performances were analyzed in terms of activation and ohmic and mass transfer overpotentials [51]. The analysis demonstrated that the degradation originated from increased activation (10–25 mV) and mass transfer (10–40 mV) losses. A growth in activation overpotential can be attributed to the decreased ECA, whereas mass transport limitation might arise from modification of the electrode structure under SO_2 exposure.

4.3. XPS analysis of SO_2 exposure to cathode catalysts

High-resolution XPS was used to study SO_2 poisoning effects on the surface chemistry of the electrodes. The elemental and chemical compositions were obtained for the reference anode and cathode as well as for exposed to SO_2 at 1.0 A cm^{-2} anode, cathode and surfaces of GDL in contact with the electrodes. The reference anode and cathodes had ~0.6 at.% of the sulfur present (Fig. 5a and b and SM 1). Exposure of the fuel cell to SO_2 resulted in a statistically significant increase in the sulfur surface concentration, with 0.83 at.% and 0.86 at.% detected at the cathode and anode, respectively. The Pt surface concentration was the same for the reference and the poisoned anode and cathode (Fig. 5a and b and SM1).

Importantly, the reference GDL also has a statistically lower surface concentration of sulfur than the poisoned one, particularly for the cathodic side (Fig. 5c, SM 1). The S grew from 0.07 to 0.18 at.% for the cathode GDL, whereas no significant change in sulfur concentration was detected on the surface of the anodic GDL. High-resolution spectra for the Pt 4f and S 2p for the studied samples are presented in Fig. 6. The shoulder on the higher binding energy is due to Pt oxides, and this shoulder increases slightly for both anodes and cathodes at the expense of a decrease in the peak due to metallic Pt (Fig. 6a and b). Fig. 5d, and SM 2 show the relative concentration of PtO for the reference and exposed materials with both the cathode and anode having statistically more oxidation detected.

The chemistry of S-species adsorbed on Pt has been studied previously [30,67,68]. In the reference cathode and anode, high valent sulfur such as sulfate and sulfite are present, contributing to peaks at 169.2 and 167.8 eV, respectively [30]. The shift to lower binding energy in the S 2p spectra for both the reference and poisoned electrodes is caused by reduction of sulfates and formation of a higher peak at 167.8 eV. Moreover, the appearance of small but detectable peaks due to elemental sulfur and sulfur coordinated to the surface of the carbon (163–164 eV) were also observed (Fig. 6c and d) [30,68]. Fig. 5e shows the surface concentration of a reduced form of S, and almost double the amount of these species is present in the poisoned electrodes versus the reference. The XPS studies of the electrodes after exposure to SO_2 clearly show formation of reduced sulfur species and elemental sulfur and support the CV results (Fig. 3a and b). Detection of elemental sulfur species at the anode suggested a possible diffusion of the contaminant or its derivative from the cathode and explained the observed excessive ECA anode loss of 11.6% compared to the reference sample (Table 1).

4.4. SO_2 impacts on ORR and PEMFC performance

The PEMFC performance under SO_2 exposure clearly showed deactivation and degradation of fuel cells. The observed SO_2 effects should be interpreted in terms of its electrochemical properties, its impacts on the Pt surface area and the oxygen reduction mechanism. Sulfur dioxide adsorption in solution on the Pt electrodes has been studied extensively
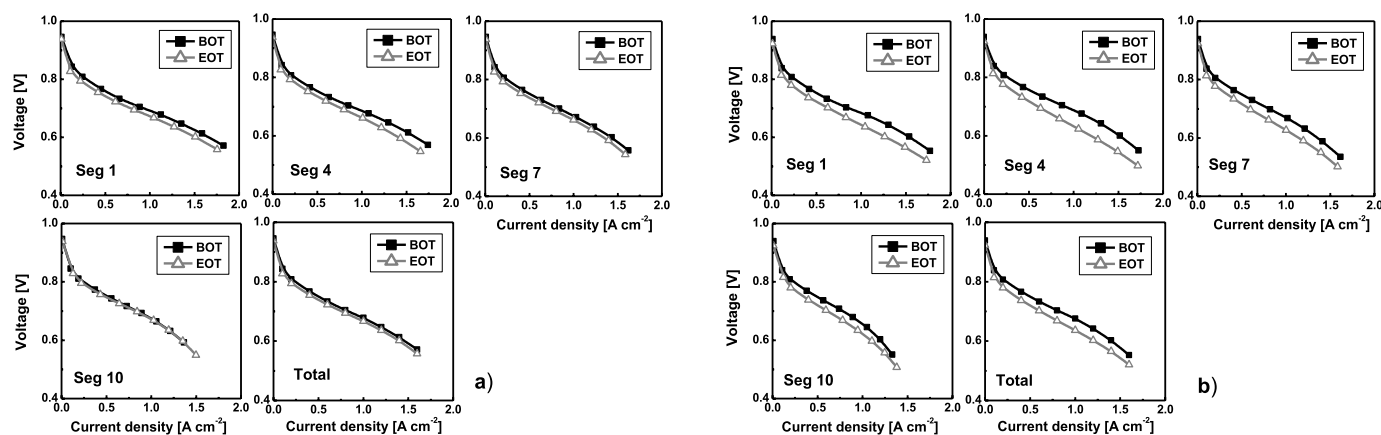

Fig. 4. VI curves for segments 1, 4, 7, 10 and for the whole cell before (BOT) and after (EOT) 2 ppm SO_2 exposure test at 0.2 (a) and 1.0 A cm^{-2} (b). Anode/cathode: H_2/air, 2/2 stoichiometry, 100/50% RH, 150/150 kPa, 80 °C.
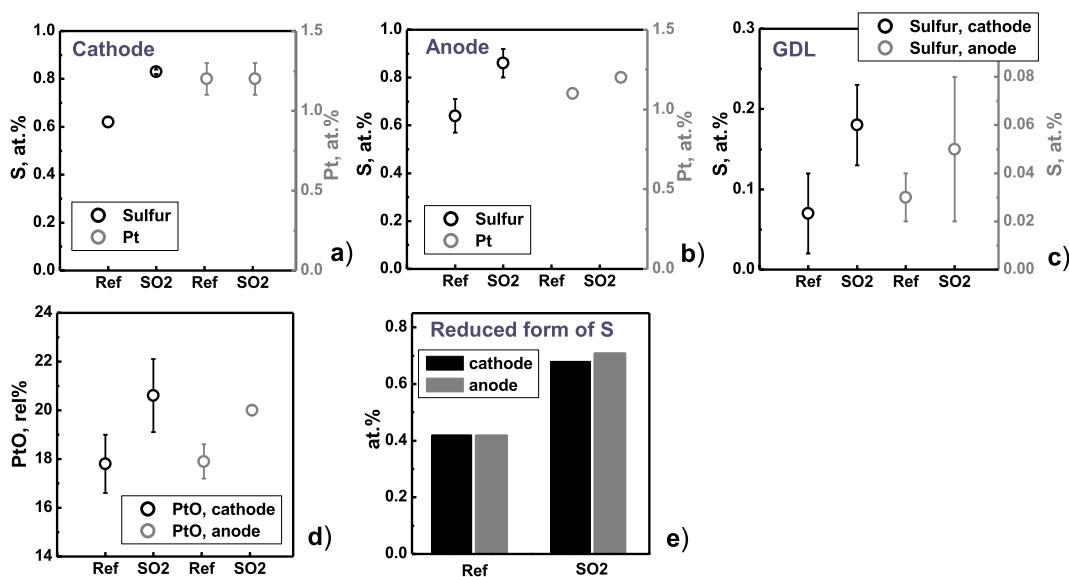
Fig. 5. Surface concentration of S and Pt for reference and exposed cathode (a), anode (b) and S surface concentration for anodic and cathodic sides of GDL (c); relative amount of PtO detected at reference and exposed cathode and anode (d); surface concentration of reduced form of S on reference and exposed cathode and anode (e).

over the last several decades [30,31,59,60,63–66,68–71]. However, the final chemistry of the adsorbates strongly depends on the electrode potential. At low potentials (0.05–0.5 V), the initially adsorbed SO_x species on Pt are reduced to zero-valent sulfur [30,62,63,65,68]. Moreover, SO_2 reduction occurred with formation of an intermediate because two reduction peaks were detected in CV [60]. The broad peak at 0.45 V was attributed to formation of SO, which was reduced to sulfur at 0.21 V. In addition, the onset for SO_2 reduction on Pt was found to be ~0.5 V. At high potential (0.8–1.4 V), S^0 and SO_x species are electrochemically oxidized to sulfates/bisulfates (SO_4^{2-}/HSO_4^-) [30,62,63,65, 68,70]. At intermediate potentials (0.5–0.8 V), the oxidation state of sulfur-containing species varies and is most likely presented by a mixture of S^0 and adsorbed SO_x [31,62,68,70].

The effects of adsorbed sulfur-containing species on oxygen reduction were previously studied using a rotating ring disk electrode methodology in Ref. [30]. The initial sulfur coverage of Pt was determined from the total charge consumed when the sulfur was oxidized from S^0 to water-soluble sulfate SO_4^{2-} at 1.3 V. Electrodes were evaluated for their ORR activity in the potential range of 0–1.0 V (vs. RHE), where the formed sulfur species (S^x) are stable. A significant 33% loss in Pt mass activity was detected when 1.2% of the Pt surface was covered by adsorbed S^x. Sulfur coverage of 14% caused a 95% loss in mass activity. The oxygen reduction pathway changed from a 4-electron to a 2-electron mechanism, leading to generation of hydrogen peroxide when 37% of the Pt surface was covered with sulfur species. The observed loss of activity with S^x coverage implies that each adsorbed S^x species blocks multiple Pt sites, perhaps by residing in the interstitial sites between atoms or even by modifications to the electronic states of neighboring Pt atoms [72]. The oxygen reduction requires adsorption and dissociation of the O_2 molecule in a bridge configuration between two adjacent Pt sites, but at high S^x coverage, there are few adjacent sites available, allowing mainly O_2 adsorption "atop" the Pt atom and leading to peroxide formation. Thus, the presence of sulfur-containing species (SO_x and S^x) on the Pt surface blocked and reduced the availability of sites for ORR as well as altered of the electronic properties of Pt. It is known that SO_2 can interact with transition metals as an σ-donor and π-acceptor. The charge transfer mechanism includes the donation of electrons from SO_2 to Pt through σ-bonds and back donation of Pt d-electrons to the anti-bonding SO_2 orbital. Evaluation of SO_2 adsorption on Pt (111) by HREELS, XPS and UPS revealed a charge transfer from Pt d-orbitals to

SO_2 [70,73]. Elemental sulfur is also known to be an electron donor in metal complexes and can act as surface modifier [59,66,70–72,74]. The presence of co-adsorbed S^x on Pt could increase the electronic density at the electrode surface and affect ORR as well as the electrochemical reactions of SO_2.

Based on analysis of our results and published data, the effects of SO_2 on PEMFC performance can be summarized in the scheme shown in Fig. 7. At the beginning of the poisoning stage, SO_2 easily adsorbs on the Pt surface, forming several types of M — SO_2 binding configurations: atop η^1 – planar/pyramidal, η^1 – S bridging, and fcc η^2 - S, O structures [70,73,75]. Adsorption of SO_2 causes loss of electrochemical surface area and negatively affects oxygen adsorption and platinum oxide formation, which results in a decrease in ORR efficiency and cell voltage.

Operation at a low current of $0.2\ A\ cm^{-2}$ led to the initial cell voltage of 0.78 V, which is rather similar to the potential of SO_2 oxidation on Pt (Fig. 7a). Therefore, it is possible to conclude that at the first hours of cell contamination, SO_2 could be predominantly oxidized on Pt, which could explain the observed delay in 3–5 h for voltage and localized current responses (Fig. 1a and b). Adsorption of SO_2 continues, forming various strongly and weakly bonded SO_x species on the Pt surface and mainly affecting inlet segments 1–4, which causes a decrease in their local performance and cell potential loss of 60 mV. However, the cell voltage under SO_2 exposure is still high (0.72 V) for SO_2 electroreduction, and thus at these conditions, we could expect SO_2 adsorption/desorption and its slow oxidation though electrochemical and possible chemical pathways [59,64,65].

PEMFC exposure to SO_2 at $1.0\ A\ cm^{-2}$ resulted in a different behavior (Fig. 1b and c and Fig. 7b). Similar to the previous case, the initial stage of contamination caused adsorption of SO_2 on Pt and a gradual decrease in ECA and the cathode potential. As soon as the cell potential reached 0.5–0.55 V, after several hours of poisoning, we observed an inflection point in the voltage profiles, a drastic local current density redistribution and formation of low-frequency inductance in the EIS curves which indicated the presence of an additional electrochemical process that involves electron transfer occurring in parallel with oxygen reduction. As shown from CV studies of SO_2 electrochemical reactions on Pt electrodes, SO_2 reduction to SO began at 0.45 V [60], and it could cause the spatial fuel cell performance similar to acetonitrile [8].

The low-frequency inductance could be attributed to the electroreduction of SO_2 to SO, which requires transfer of two electrons and
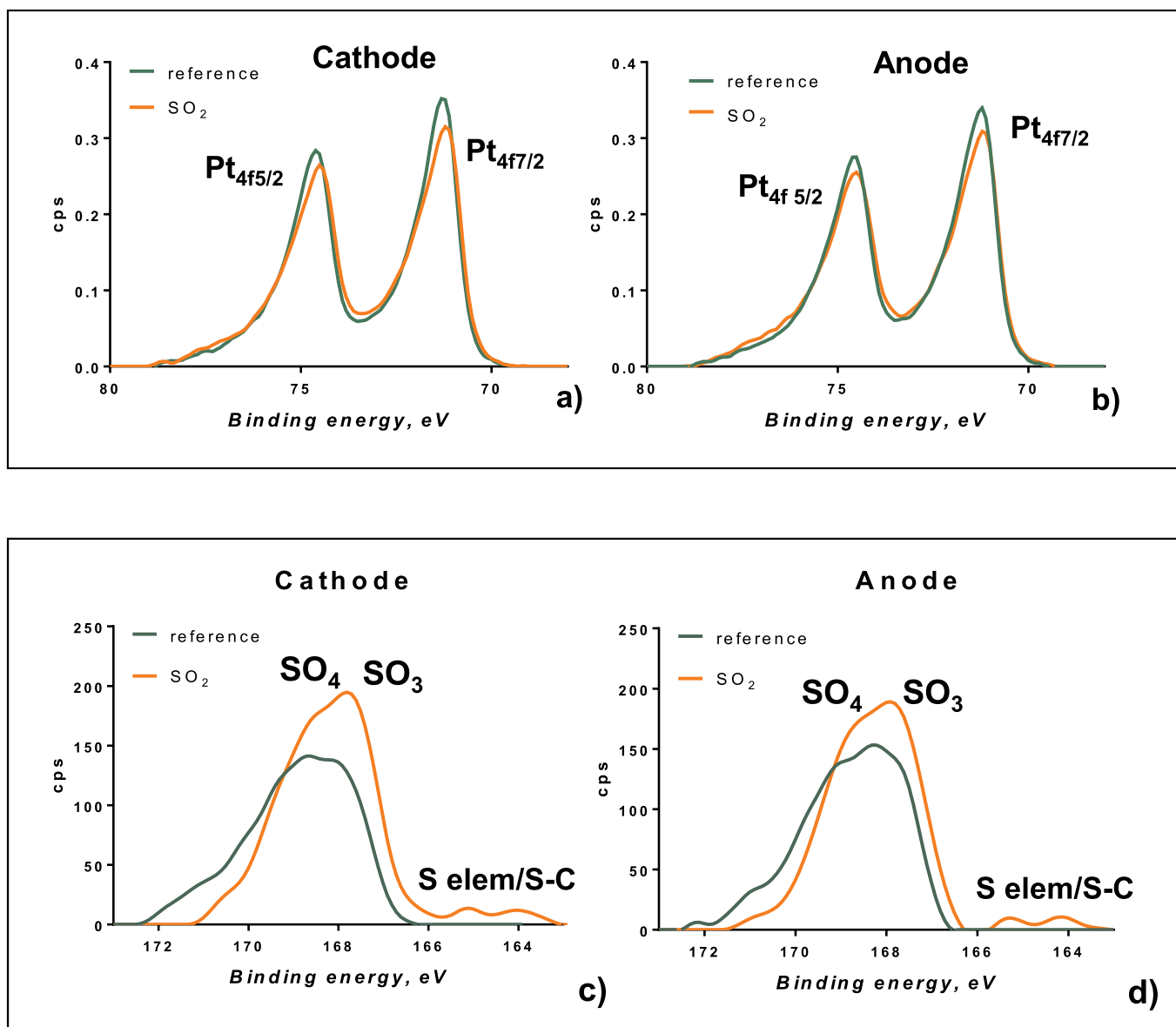
Fig. 6. High-resolution Pt 4f spectrum for cathode (a) and anode (b); S 2p for cathode (c) and anode (d).

could occur in several steps. However, we cannot rule out that the consecutive SO reduction to S could be an explanation for the EIS inductive loops. A comparison of the reduction potentials of 0.45 and 0.21 V for SO_2 reduction on Pt in aqueous solutions at room temperature, with 0.5–0.525 V obtained for PEMFC operation, is quite challenging due to different operating conditions. Nerveless, these values gave us general ideas about possible SO_2 reactions. Further SO_2 cathode poisoning led to a gradual cell voltage drop to 0.37 V. Thus, different SO_2 electrochemical reactions occurring at high and low current altered the PEMFC behavior patterns and resulted in accumulation of sulfur-containing species on the Pt surface to a greater extent for $1.0 \, A \, cm^{-2}$ than operation at $0.2 \, A \, cm^{-2}$, which is confirmed by CV (Fig. 3a and b).

Self-recovery did not restore the initial performance, most likely due to the existence of strongly adsorbed SO_x species for $0.2 \, A \, cm^{-2}$ and formation of zero-valent sulfur for $1.0 \, A \, cm^{-2}$. From a practical point of view, any recovery procedure should consider the constraints of operating PEMFCs, which include the fuel cell stack, limited gas supply for the anode and cathode (only hydrogen and air), pumps, humidifiers and power electronics. The main approach to restoring fuel cell performance is to remove any sulfur-containing species from the Pt surface, which can

be achieved by potential cycling of the cathode to a potential greater than 1.0 V to oxidize S^0. Other recovery strategies such as several successive VI measurements or an increase in air flow were also studied [32, 35], but the potential cycling proposed in Ref. [33] demonstrated the best results (99% recovery) with time requirements of under 3 min.

4.5. Modeling the SO_2 mechanism of PEMFC poisoning

Analysis of the published literature showed that a significant difference exists between reaction mechanisms proposed in experimental articles such as [32,40] and mechanisms proposed for modeling purposes [47–49]. The first category generally suggests simple mechanisms that omit any additional intermediates: this, as argued in the last sections, does not allow to describe the complex behavior observed. The latter category commonly proposes quite complex mechanisms. E.g., in Ref. [48] three different adsorptions paths of the contaminant are modeled. It is possible that there are different paths, and the complex mechanisms are difficult to parameterize, which impedes to interpret the results and determine the dominant process. In the following, we would like to present with a comparison of three mechanisms of
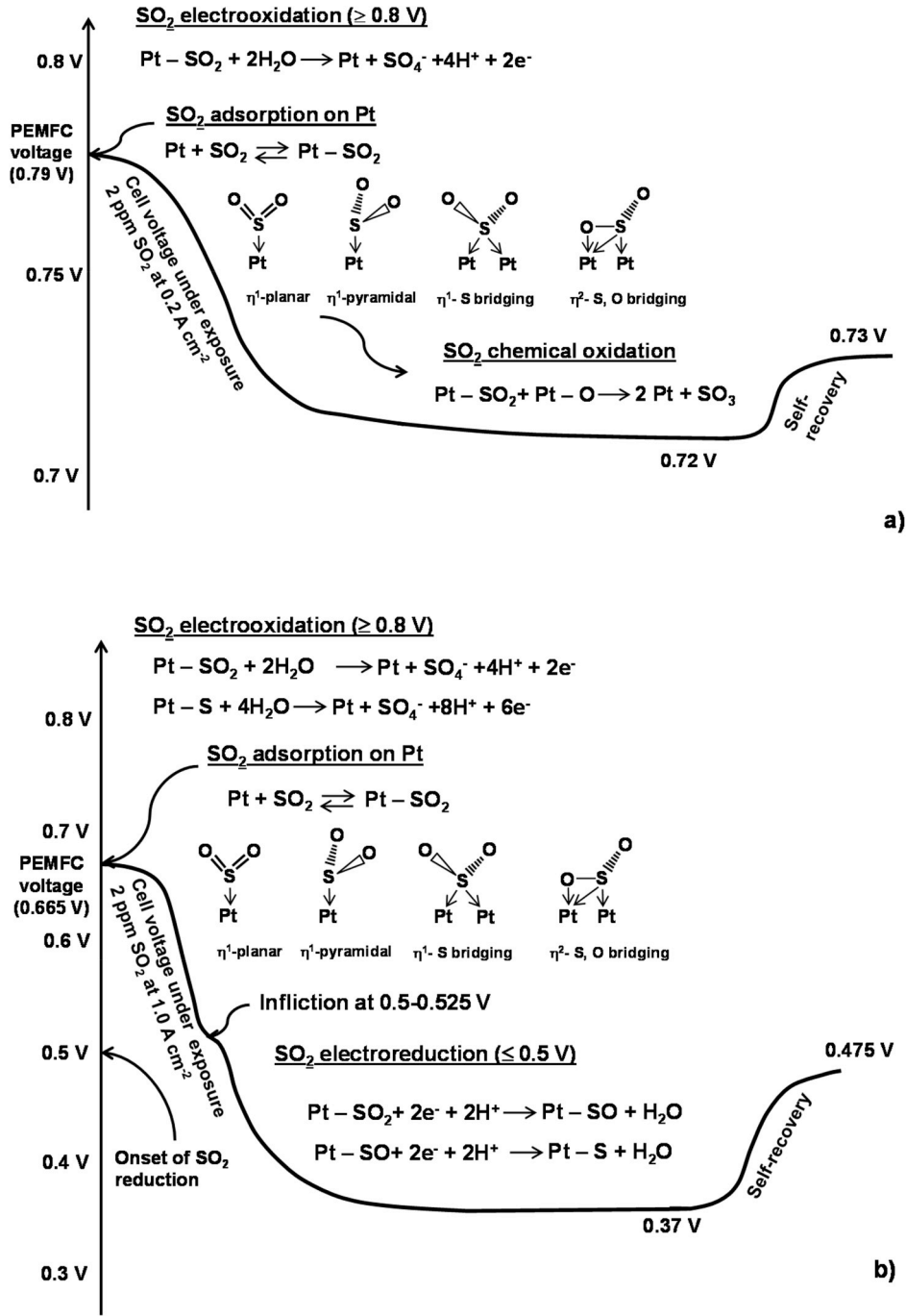
Fig. 7. Schematic of possible SO_2 processes in PEMFC operation at 0.2 (a) and $1.0\,A\,cm^{-2}$ (b).

increasing complexity and amount of reaction species, how sorption, reversible electrochemical reactions and irreversible steps interact and impact the deactivation, reactivation and poisoning behavior. The mechanisms consider the chemical and electrochemical reactions discussed in the literature and those identified with our experimental data. By comparison of simulation to experiment, the analysis reveals the most likely mechanism, and helps to understand and possibly mitigate contamination of the Pt cathode by SO_2.

All three mechanisms contain a simple one-step oxygen reduction (10) of priory adsorbed oxygen (Eq. (9)) and subsequent desorption of water (11):

$$O_2 + [\ ] \rightleftharpoons O_2^* \tag{9}$$

$$O_2^* + [\ ] + 4H^+ + 4e \rightleftharpoons 2H_2O^* \tag{10}$$

$$H_2O + [\ ] \rightleftharpoons H_2O^* \tag{11}$$

In a first sorption-only model, we only include the SO_2 adsorption on Pt with formation of a weakly (SO_2^*) and a strongly adsorbed species (SO_2^{**}) (Eqs. (12) and (13)):

$$SO_2 + [\ ] \rightleftharpoons SO_2^* \tag{12}$$

$$SO_2^* + [\ ] \rightleftharpoons SO_2^{**} \tag{13}$$
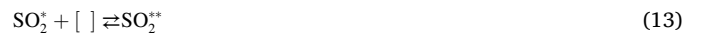
Square brackets denote a free surface site, an asterisk denotes an adsorbed state and a double asterisk denotes a strong adsorbed state occupying two surface sites. This mechanism contains only reversible

steps and would allow to simulate deactivation, including de-facto poisoning by a more strongly adsorbed intermediate.

A second sorption-electrochemical model contains besides these two adsorbed SO_2 species also the electrochemical reduction of SO_2 to $SO*$ and $S*$ (Eqs. (14) and (15)):

$$SO_2^{**} + 2H^+ + 2e \rightleftarrows SO^* + H_2O + [\ ] \tag{14}$$

$$SO^* + 2H^+ + 2e \rightleftarrows S^* + H_2O \tag{15}$$

Both steps are reversible, i.e. the sulfur species may be oxidized again. This model also allows us to bring in potential dependence of the SO_2 processes at the surface.

In the full model, we assume additionally the chemical production of SO_3^{2-} species that can be removed from the Pt surface (Eqs. (16) and (17)) [60–62]:

$$SO_2^* + H_2O^* \rightarrow SO_3^{2\ *} + 2H^+ \tag{16}$$

$$SO_3^{2\ *} \rightarrow SO_3^{2} + [\ ] \tag{17}$$

Chemical reaction 16 and the dissolution of its product (Eq. (17)) are the only irreversible processes. The proposed mechanism is strongly based on the experimental findings in Section 4.1 and conclusions illustrated in Fig. 7.

A general reaction kinetics scheme is formulated in Eq. (2). For the reaction mechanism introduced by Eqs. (9)–(17), the respective kinetics are described as follows:

$$r_{O_2,ads} \quad k_{f,9}\frac{c_{O_2}}{c_{O_2,0}}\Theta \quad k_{b,9}\Theta_{O_2^*}, \tag{18}$$

$$r_{ORR} \quad k_{f,10}\Theta_{O_2^*}\Theta \exp\left(\alpha\frac{F}{RT}\eta\right) \quad k_{b,10}\Theta_{H_2O^*}^2 \exp\left((1 \quad \alpha)\frac{F}{RT}\eta\right), \tag{19}$$

$$r_{H_2O,ads} \quad k_{f,11}\Theta \quad k_{b,10}\Theta_{H_2O^*}. \tag{20}$$

$$r_{SO_2,ads,1} \quad k_{f,12}\frac{c_{SO_2}}{c_{SO_2,0}}\Theta \quad k_{b,12}\Theta_{SO_2^*}, \tag{21}$$

$$r_{SO_2,ads,2} \quad k_{f,13}\Theta_{SO_2^*}\Theta \quad k_{b,13}\Theta_{SO_2^{**}}, \tag{22}$$

$$r_{SO_2,dis,1} \quad k_{b,14}\Theta_{SO^*}\Theta\Theta_{H_2O} \exp\left(\alpha\frac{F}{RT}\eta\right) \quad k_{f,14}\Theta_{SO_2^{**}}\exp\left((1 \quad \alpha)\frac{F}{RT}\eta\right), \tag{23}$$

$$r_{SO_2,dis,2} \quad k_{b,15}\Theta_{S^*}\Theta_{H_2O} \exp\left(\alpha\frac{F}{RT}\eta\right) \quad k_{f,15}\Theta_{SO^*} \exp\left((1 \quad \alpha)\frac{F}{RT}\eta\right), \tag{24}$$

$$r_{SO_2,side} \quad k_{f,16}\Theta_{SO_2^*}\Theta_{H_2O}, \tag{25}$$

$$r_{SO_3^2,des} \quad k_{f,17}\Theta_{SO_3^2}, \tag{26}$$

Activities of protons and water are assumed to be one in Eq. (18)–(26) and Θ is the surface coverage of free surface sites. Kinetic constants were estimated from the experiments, partially on a coarse grid, and partially by applying a least square solver. This approach is in accordance with, e.g., the work of Shi et al. [48] and Mao and Krewer [76]. The adjusted parameters were k_f of Eqs. (12)–(16) and k_b of Eqs. (12), (13) and (15) for SO_2 as well as 10 and 11 for ORR. The least-squares formulation of parameter estimation is shown in Eq. (27). The estimated parameters are ζ and ϵ, the latter is the deviation between the experiment and simulation which is minimized.

$$\min_{\zeta} \epsilon : \epsilon(\zeta) \quad \sum_i \left(E_{cell,sim}(\zeta,t_i) \quad E_{cell,exp}(t_i) \right)^2 \tag{27}$$

The kinetic rate constant of the ORR was estimated first, facilitating the SO_2-free parts of the experiment and the VI curve. Consecutively, the

SO_2 kinetics were estimated. Due to the structural unidentifiability of the model, it is not possible to estimate the entire parameter set from the experiment. The resulting kinetic constants are listed in Table 2. Additionally, the mass transfer coefficients of SO_2 in the ionomer phase were estimated from the experiment to $0.0038\ \mathrm{s^{-1}}$, which is approximately a quarter of the value for O_2 measured in Ref. [50]. Because different formulations of the reaction mechanism lead to different kinetic constants, the parameters of the model can only be compared with the literature for a subset of parameters. For instance, oxygen adsorption is a common element of the models in the literature. For example, Shi et al. stated a ratio of the forward and backward reaction constants of oxygen adsorption of $5.8\cdot10^4\ \mathrm{cm^3\ mol^{-1}}$ [48]. Under steady state conditions, a respective quantity $k_f/(k_b \cdot c_{ref})$ from Eq. (24) can be derived and is equal to $2.7\cdot10^4\ \mathrm{cm^3\ mol^{-1}}$ for a reference concentration of $36.57\ \mathrm{mol\ m^{-3}}$ (ideal gas at cell temperature) and the kinetic constants listed in Table 2. Thus, our assumption of $k_f \quad k_b$ leads to a value close to that of the literature.

To further fortify the plausibility of the estimated parameter set, simulated VI curves are shown in SM 3. The model reproduces activation losses and the linear ohmic range of the experimental cell in quantitative accordance. The onset of the diffusion range in the experiment is not visible in the simulations due to the neglect of diffusion in the GDL. Further, the spread of segment currents qualitatively fits the experiments, with a higher current density in the inlet segment compared with the outlet segment.

In a first step, we consider the simplest mechanism, where SO_2 is only able to adsorb and desorb without chemical or electrochemically reactions occurring. Fig. 8a and b shows the simulation results along the experimental data for the pathway considering ORR and reversible SO_2 adsorption with the formation of weakly and strongly adsorbed species SO_2* and SO_2** (Eqs. (12) and (13)). The SO_2 introduction into the air stream leads to a steep voltage decrease for the simulation and experimental data (Fig. 8a). At approximately 0.4 V, a voltage plateau is reached, and the voltage remains unchanged until SO_2 injection is stopped. At the recovery stage, the voltage increases for the simulations and experiments until a further plateau is reached. However, the simulated surface coverage data show that SO_2 is continuously removed from the surface (Fig. 8b), so that even if this process is slow, sooner or later the original performance before SO_2 exposure will be reached. This is indeed expected, as the sorption processes are reversible. At the low voltage plateau, a high fraction of the surface is covered by the adsorbed SO_2, which leads to a depletion of oxygen adsorbed species for ORR and thus to the voltage drop. In conclusion, SO_2 adsorption is able to cause the voltage drop, but it is reversible, and hence, a potentially irreversible step, such as a reversible electrochemical reaction triggered by potential, must be added to the mechanism to explain our experimental data.

In the second model therefore, SO_2 electrochemical reduction (Eqs. (14) and (15)) is added to the mechanism, as is commonly suggested as the irreversible process of SO_2 poisoning. In this case, the reduction leads to a voltage decay till the lower cutoff voltage is reached (Fig. 8c, orange curve). This situation is related to surface blockage due to the produced sulfur species $SO*$ and $S*$. Their influence will not be discussed separately, as they have the same effect and the kinetics between both

Table 2
Values of kinetic constants used in the simulation.

Reaction	Forward $k_{f,i}$ [mol m ^{2} s ^{1}]	Backward $k_{b,i}$ [mol m ^{2} s ^{1}]
Eq. 9	10^9	10^9
Eq. 10	10^{-3}	$2.4\cdot10^{\ 6}$
Eq. 11	1	1.2
Eq. 12	0.20	$3.6\cdot10^{\ 8}$
Eq. 13	$2.4\cdot10^{\ 8}$	$7.3\cdot10^{\ 10}$
Eq. 14	$2.0\cdot10^{\ 7}$	$2.0\cdot10^{\ 6}$
Eq. 15	$2.0\cdot10^{\ 7}$	$6.2\cdot10^{\ 9}$
Eq. 16	$1.0\cdot10^{\ 8}$	0
Eq. 17	10^{-9}	0
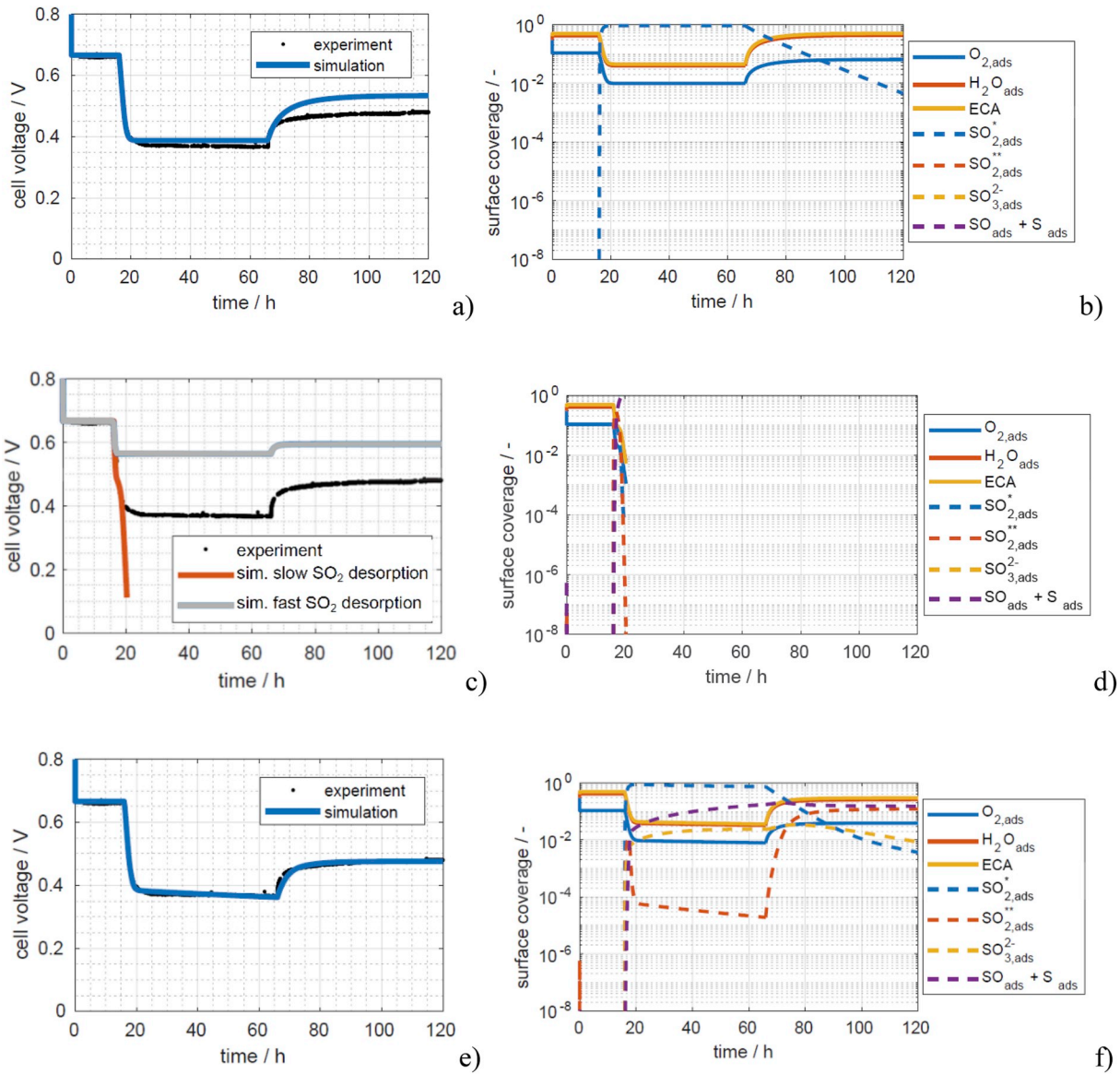
Fig. 8. Cell voltage (a, c, e) and surface coverage (b, d, f) vs. time at a current of $1.0\,A\,cm^{-2}$ and 2 ppm SO_2. The sorption-only reaction mechanism includes ORR and reversible SO_2 adsorption (Eqs. (12) and (13)) (a, b). The sorption-electrochemistry pathway takes into account ORR, reversible SO_2 adsorption and electrochemical reduction of SO_2 to SO^* and S^* (Eqs. (12)–(15)) no limiting intermediates) (c, d). Graph d) refers to the scenario of the orange line in the plot c). Full reaction mechanism including sorption, electrochemical and chemical reactions (Eqs. (12)–(17)) (e, f). (For interpretation of the references to colour in this figure legend, the reader is referred to the Web version of this article.)

species cannot be identified with our present experimental set. The transition between the voltage decay due to reversible SO_2 adsorption (Eqs. (12) and (13)) and SO_2 reduction (Eqs. (14) and (15)) is indicated by an inflection point in the orange voltage curve at ~0.5 V. This inflection point was also observed in experimental data (Fig. 1 c, d). At that potential the reduction reactions are triggered, leading to a further decrease of desorbing sulfur species, which in turn further decreases potential. Fig. 8d illustrates the rapid increase of the poisoning species including the autocatalytic effect with all adsorbed SO_2 reacting to SO^* or S^* which leads to the potential drop (Fig. 8c, orange curve). In case, the desorption of $SO_2^* k_{b,12}$ is sufficiently accelerated to a values of $3.6 \cdot 10^{-6}\,mol\,m^{-2}\,s^{-1}$ compared to $3.6 \cdot 10^{-8}\,mol\,m^{-2}\,s^{-1}$ in the standard parameter set to prevent the autocatalytic reaction (see gray line in Fig. 8c). Due to this, a higher voltage plateau is reached, and with it a similar behavior as for the sorption-only mechanism takes place. Such a case that the electrochemical reduction is not triggered has been observed in the PEMFC performance exposed to SO_2 at low current

operation (Fig. 1a). These results indicate that the mechanism of SO_2 adsorption with direct electrochemical reduction is not feasible to explain the experimental findings at high current operation. Either the reduction is not triggered, leading to reversible surface blockage, or SO_2 reduction is triggered, causing continuously accelerated degradation until the lower cutoff voltage is reached.

To overcome this limitation, some adsorbed species must be able to react further to free surface sites for ORR. As a consequence, the full reaction mechanism of Eqs. (12)–(17) including chemical reactions and desorption are applied. Fig. 8e and f presents the simulated voltage response and the corresponding surface coverages of the different adsorbed species. The simulation provides a qualitatively and quantitatively accurate reproduction of the PEMFC behavior when poisoned by SO_2 at $1.0\,A\,cm^{-2}$ (Fig. 1c). In a first step, the SO_2 adsorption partially suppresses the ORR reactants from the Pt surface, leading to a decrease in potential. In parallel, the strongly adsorbed SO_2^{**} species are formed before the electroreduction products SO^* and S^* are built.

Electrochemical reduction of the adsorbed SO_2 species is triggered by the low potential of ~0.5–0.525 V. The produced SO* and S* compete and inhibit the formation of SO_2** as well as the ORR reactants. Suppression of SO_2** formation subsequently leads to the steady voltage plateau as the electroreduction suppresses its own reactant. At recovery, SO_2* and SO_2** are removed from the surface. The reduced products SO* and S* remain at the surface due to the low cell potential and the higher steady state potential of electrooxidation.

Concluding this section, a simulation-based reaction mechanism is found, which is able to quantitatively explain the voltage response of the PEMFC to SO_2 poisoning, which was investigated experimentally in Section 4.1 (Fig. 1) and discussed in details in Section 4.4 (Fig. 7). This result offers an additional intermediate SO_2**. The depletion of this species at low potentials due to SO*/S* formation leads to a stabilization and steady state of the cell performance at a lower potential plateau. The mechanism is applicable for the poisoning step as well as for recovery.

5. Conclusions

The negative effects of SO_2 in the air stream on localized PEMFC performance and durability were studied using a segmented cell system, electrochemical methods and XPS. It was demonstrated that 2 ppm SO_2 caused voltage drops of 60 and 295 mV for a fuel cell operated under constant current holds of 0.2 and 1.0 A cm^{-2}, respectively. Moreover, the PEMFC did not restore its initial performance under self-recovery conditions when SO_2 injection into the air stream was stopped. These electrochemical tests were simulated applying a physics-based model to support the experimental findings. CV and XPS studies showed that this lack of self-recovery is caused by the formation of adsorbed elemental sulfur on the Pt surface originating from the reduction of SO_2 at fuel cell operating potentials. Only cyclic voltammetry resulted in S^0 oxidation at potentials higher than 1.2 V and Pt surface recovery. However, SO_2 exposure led to a cathode ECA decrease of 18–22%, which caused irreversible performance losses of 20–30 and 25–50 mV for low and high current density operating conditions. Application of the physics-based mathematical model simulation revealed a complex interplay of SO_2 adsorption, electrochemical reduction to a species like SO* and S* and sufficient surface site freeing due to a chemical reaction allows stabilization of the poisoned cell at a low voltage.

Acknowledgements

References

[1] J.M. Moore, P.L. Adcock, J.B. Lakeman, G.O. Mepsted, The effects of battlefield contaminants on PEMFC performance, J. Power Sources 85 (2000) 254.

[2] O.A. Baturina, Y. Garsany, B.D. Gould, K.E. Swider-Lyons, in: H. Wang, H. Li, X.-Z. Yuan (Eds.), PEM Fuel Cell Failure Mode Analysis, CRC Press, 2011, pp. 199–241.

[3] F.H. Garzon, F.A. Uribe, Effects of contaminants of catalyst activity, in: W. Vielstich, H.A. Gasteiger, A. Lamm, H. Yokokawa (Eds.), Handbook of Fuel Cells X. Fundamentals, Technology and Applications, Vol. 5. Advances in Electrocatalysis, Materials, Diagnostics and Durability, John Wiley & Sons, 2010.

[4] N. Zamel, X. Li, Effect of contaminants on polymer electrolyte membrane fuel cells, Prog. Energy Combust. Sci. 37 (2011) 292.

[5] J. St-Pierre, Y. Zhai, M. Angelo, Effect of selected airborne contaminants on PEMFC performance, J. Electrochem. Soc. 161 (2014) F280.

[6] A. Talke, U. Misz, G. Konrad, A. Heinzel, D. Klemp, R. Wegener, Influence of urban air on PEMFC vehicles – long term effects of air contaminants in an authentic driving cycle, J. Power Sources 400 (2018) 556.

[7] T.V. Reshetenko, J. St-Pierre, Study of acetylene poisoning of Pt cathode on proton exchange membrane fuel cell spatial performance using a segmented cell system, J. Power Sources 287 (2015) 401.

[8] T.V. Reshetenko, J. St-Pierre, Study of acetonitrile poisoning of Pt cathode on proton exchange membrane fuel cell spatial performance using a segmented cell system, J. Power Sources 293 (2015) 929.

[9] T.V. Reshetenko, J. St-Pierre, Study of the aromatic hydrocarbons poisoning of platinum cathodes on proton exchange membrane fuel cell spatial performance using a segmented cell system, J. Power Sources 333 (2016) 237.

[10] T.V. Reshetenko, J. St-Pierre, Effects of propylene, methyl methacrylate and isopropanol poisoning on spatial performance of a proton exchange membrane fuel cell, J. Power Sources 378 (2018) 216.

[11] T.V. Reshetenko, K. Artyushkova, J. St-Pierre, Spatial proton exchange membrane fuel cell performance under bromomethane poisoning, J. Power Sources 342 (2017) 135.

[12] C. Jia, S. Batterman, C. Godwin, VOCs in industrial, urban and suburban neighborhoods. Part 1: Indoor and outdoor concentrations, variations and risk drivers, Atmos. Environ. 42 (2008) 2083.

[13] S.A. Yvon-Lewis, E.S. Saltzman, S.A. Montzka, Recent trends in atmospheric methyl bromide: analysis of post-Montreal Protocol variability, Atmos. Chem. Phys. 9 (2009) 5963.

[14] D. Schwela, O. Zali, Urban Traffic Pollution, E&FN Spon, London, New York, 1999.

[15] J. Xu, Y. Gao, Sh Uchiyama, T. Sodesawa, Analysis of volatile organic compounds (VOCs) in the urban atmosphere of Beijing, J. Chem. Eng. Jpn. 41 (2008) 997.

[16] H. Li, J. Zhang, K. Fatih, Z. Wang, Y. Tang, Z. Shi, S. Wu, D. Song, J. Zhang, N. Jia, S. Wessel, R. Abouatallah, N. Joos, PEMFC contamination: testing and diagnosis of toluene-induced cathode degradation, J. Power Sources 185 (2008) 272.

[17] J. St-Pierre, M. Virji, Cell performance distribution in a low-temperature proton exchange membrane fuel cell stack during propene contamination, J. Appl. Electrochem. 46 (2016) 169.

[18] O. Baturina, A. Epsteyn, P. Northrup, K. Swider-Lyons, The influence of cell voltage on the performance of a PEM fuel cell in presence of HCl in air, J. Electrochem. Soc. 161 (2014) F365.

[19] M.S. Angelo, J. St-Pierre, The effect of common airborne impurities and mixtures on PEMFC performance and durability, ECS Trans 64 (2014) 773.

[20] D. Imamura, E. Yamaguchi, Effect of air contaminants on electrolyte degradation in PEMFC, ECS Trans 25 (2009) 813.

[21] Y. Nagahara, S. Sugawara, K. Shinohara, The impact of air contaminants on PEMFC performance, J. Power Sources 182 (2008) 422.

[22] R. Mohtadi, W.-K. Lee, J.W. Van Zee, Assessing durability of cathodes exposed to common air impurities, J. Power Sources 138 (2004) 216.

[23] F. Jing, M. Hou, W. Shi, J. Fu, H. Yu, P. Ming, B. Yi, The effect of ambient contamination on PEMFC performance, J. Power Sources 166 (2007) 172.

[24] X.-Z. Yuan, H. Li, Y. Yu, M. Jiang, W. Qian, S. Zhang, H. Wang, S. Wessel, T.T. H. Cheng, Diagnosis of contamination introduced by ammonia at the cathode in a PEMFC, Int. J. Hydrogen Energy 37 (2012) 12464.

[25] D. Yang, J. Ma, L. Xu, M. Wu, H. Wang, The effect of nitrogen oxides in air on the performance of PEMFC, Electrochim. Acta 51 (2006) 4039.

[26] M. Bétournay, G. Bonnell, E. Edwardson, D. Paktunc, A. Kaufman, A.T. Lomma, The effect of mine conditions on the performance of a PEM fuel cell, J. Power Sources 134 (2004) 80.

[27] Y.-G. Yoon, I. Choi, C.-H. Lee, J. Han, H.-J. Kim, E.-A. Cho, S.J. Yoo, S.W. Nam, T.-H. Lim, J.J. Yoon, S. Park, J.H. Jang, Systematic analysis for the effects of atmospheric pollutants in cathode feed on the performance of proton exchange membrane fuel cells, Bull. Korean Chem. Soc. 35 (2014) 3475.

[28] P. Faber, F. Drewnick, J. Piske, T. Kurtz, S. Borrmann, Effects of atmospheric aerosol on the performance of environmentally sustainable pssive air-breathing PEM fuel cells, Int. J. Hydrogen Energy 37 (2012) 17203.

[29] A.A. Franco, M. Barthe, L. Rouillon, O. Lemaire, Mechanistic investigations of NO₂ impact on ORR in PEM fuel cells: a coupled experimental and multi-scale modeling approach, ECS Trans 25 (2009) 1595.

[30] Y. Garsany, O.A. Baturina, K.E. Swider-Lyons, Impact of SO₂ on the oxygen reduction reaction at Pt/Vulcan carbon electrocatalysts, J. Electrochem. Soc. 154 (2007) B670.

[31] O.A. Baturina, K.E. Swider-Lyons, Effect of SO₂ on the performance of the cathode of a PEM fuel cell at 0.5-0.7 V, J. Electrochem. Soc. 156 (2009) B1423.

[32] B.D. Gould, O.A. Baturina, K.E. Swider-Lyons, Deactivation of Pt/VC PEMFC cathodes by SO₂, H₂S and COS, J. Power Sources 188 (2009) 89.

[33] B.D. Gould, G. Bender, K. Bethune, S. Dorn, O.A. Baturina, R. Rocheleau, K. E. Swider-Lyons, Operational performance recovery of SO₂ contaminated PEMFCs, J. Electrochem. Soc. 157 (2010) B1569.

[34] J. Fu, M. Hou, C. Du, Z. Shao, B. Yi, Potential dependence of SO₂ poisoning and oxidation at the cathode of PEMFCs, J. Power Sources 187 (2009) 32.

[35] P. Jayaraj, P. Karthika, N. Rajalakshmi, K.S. Dhathathreyan, Mitigation studies of sulfur contaminated electrodes for PEMFC, Int. J. Hydrogen Energy 39 (2014) 12045.

[36] S. Tsushima, K. Kaneko, S. Hirai, Two-stage degradation of PEMFC performance due to sulfur dioxide contamination, ECS Trans 33 (2010) 1645.

[37] S. Tsushima, K. Kaneko, H. Morioka, S. Harai, Influence of SO₂ concentration and relative humidity on electrode poisoning in PEMFC, J. Therm. Sci. Technol. 7 (2012) 619.

[38] J.A. Prithi, B.S. Viswanath, N. Rajalakshmi, K.S. Dhathathreyan, Stadies on PEMFC stack for SO₂ contamination at air cathode, Fuel Cells 17 (2017) 308.

[39] M.M. Saleh, M.I. Awad, F. Kitamura, T. Ohsaka, Sulphur dioxide poisoning and recovery of Pt nanoparticles: effect of particle size, Int. J. Electrochem. Sci. 7 (2012) 12004.

[40] Y. Zhai, G. Bender, S. Dorn, R. Rocheleau, The multiprocess degradation of PEMFC performance due to SO_2 contamination and its recovery, J. Elcetochem. Soc. 157 (2010) B20.

[41] K.-C. Lum, S.-L. Ng, W.-C. Hui, P.-K. Chan, Enviromental quality of urban parks and open spaces in Hong Kong, Environ. Monit. Assess. 111 (2005) 55.

[42] Annual Summary – Hawaii Air Quality Data, 2015. https://health.hawaii.gov/cab/files/2016/12/aqbook_2015.pdf.

[43] A.J. Sutton, T. Elias, R. Navarrete, Volcanic Gas Emissions and Their Impact on Ambient Air Character at Kilauea Volcano, Hawaii, Open-File Report 94-569, 1994. https://digital.library.unt.edu/ark:/67531/metadc707134/.

[44] E. Tam, R. Miike, S. Labrenz, A.J. Sutton, T. Elias, J. Davis, Y.-L. Chen, K. Tantisira, D. Dockery, E. Aval, Volcanic air pollution over the Island of Hawaii: emissions, dispersal and composition. Association with respiratory symptoms and lung function in Hawaii Island school children, Environ. Int. 92–93 (2016) 543.

[45] D. Hagan, G. Isaacman-Van Wertz, J.P. Franklin, L.M.M. Wallace, B.D. Kocar, C. L. Heald, J.H. Kroll, Calibration and assessment of electrochemical air quality sensors by co-location with regulatory-grade instruments, Atmos. Meas. Tech. 11 (2018) 315.

[46] T.V. Reshetenko, K. Bethune, M.A. Rubio, R. Rocheleau, Study of low concentration CO poisoning of Pt anode in a proton exchange membrane fuel cell using spatial electrochemical impedance spectroscopy, J. Power Sources 269 (2014) 344.

[47] Z. Shi, D. Song, J. Zhang, Z.-S. Liu, S. Knights, R. Vohra, N. Jia, D. Harvey, Transient analysis of H_2S contamination on the performance of PEM fuel cell, J. Electrochem. Soc. 154 (2007) B609.

[48] Z. Shi, D. Song, H. Li, K. Fatih, Y. Tang, J. Zhang, Z. Wang, S. Wu, Z.-S. Liu, H. Wang, J. Zhang, A general model for air-side PEMFC contamination, J. Power Sources 186 (2009) 435.

[49] J. St-Pierre, PEMFC contamination model: Competitive adsorption followed by surface segregated electrochemical reaction leading to an irreversibly adsorbed product, J. Power Sources 195 (2010) 6379.

[50] T.V. Reshetenko, J. St-Pierre, Separation method for oxygen mass transport coefficient in gas and ionomer phases in PEMFC GDE, J. Electrochem. Soc. 161 (2014) F1089.

[51] T.V. Reshetenko, G. Bender, K. Bethune, R. Rocheleau, Systematic study of back pressure and anode stoichiometry effects on spatial PEMFC performance distribution, Electrochim. Acta 56 (2011) 8700.

[52] T.V. Reshetenko, G. Bender, K. Bethune, R. Rocheleau, A segmented cell approach for studying the effects of serpentine flow field parameters on PEMFC current distribution, Electrochim. Acta 88 (2013) 571.

[53] R.D. Harington, M. Henderson, Impedance plane display of a reaction with an adsorbed intermediate, J. Electroanal. Chem. 39 (1972) 81.

[54] D.A. Harrington, B.E. Conway, AC impedance of faradaic reactions involving electrosorbed intermediates – I. Kinetic theory, Electrochim. Acta 32 (1987) 1703.

[55] Chu-Nan Cao, On the impedance plane displays for irreversible electrode reactions based on the stability conditions of the steady-state. I. One state variable besides electrode potential, Electrochim. Acta 35 (1990) 831.

[56] J.-P. Diard, B. Le Gorrec, C. Montella, Calculation, simulation and interpretation of electrochemical impedances. Part 3. Conditions for observation of low frequency inductive diagrams for a two-step electron transfer reaction with an adsorbed intermediate species, J. Electroanal. Chem. 326 (1992) 13.

[57] P. Córdoba-Torres, M. Keddam, R.P. Nogueira, On the intrinsic electrochemical nature of the inductance in EIS. A Monte Carlo simulation of the two-consecutive-step mechanism: the flat surface 2 D case, Electrochim. Acta 54 (2008) 518.

[58] U. Krewer, M. Christov, T. Vidakovic, K. Sundmacher, Impedance spectroscopic analysis of the electrochemical methanol oxidation kinetics, J. Electroanal. Chem. 589 (2006) 148.

[59] T. Loučka, Adsorption and oxidation of Sulphur and of Sulphur dioxide at the platinum electrode, Electroanal. Chem. Interfacial Electrochem. 31 (1971) 319.

[60] A.Q. Contractor, H. Lal, The nature of species adsorbed on Pt from SO_2 solutions, J. Electroanal. Chem. 93 (1978) 99.

[61] A.Q. Contractor, H. Lal, Two forms of chemisrbed sulfur on Pt and related species, J. Electroanal. Chem. 96 (1979) 175.

[62] O. Baturina, B.D. Gould, A. Korovina, Y. Garsany, R. Stroman, P.A. Northrup, Products of SO_2 adsorption on fuel cell electrocatalysts by combination of sulfur K-edge XANES and electrochemistry, Langmuir 27 (2011) 14930.

[63] C. Quijada, A. Rodes, J.L. Vázquez, J.M. Pérez, A. Aldaz, Electrochemical behavior of aqueous SO_2 on Pt electrodes in acidic medium. A voltammetric and in situ Fourier transform IR study.Part I. Oxidation of SO_2 on Pt electrodes with Sulphur-oxygen adsorbed species, J. Electroanal. Chem. 394 (1995) 217.

[64] A.J. Appleby, B. Pichon, The mechanism of the electrochemical oxidation of SO_2 in sulfuric acid solutions, J. Electroanal. Chem. 95 (1979) 59.

[65] C. Korzeniewski, W. McKenna, S. Pons, An in situ infrared study of the oxidation of sulfur dioxide on platinum electrodes, J. Electroanal. Chem. 235 (1987) 361.

[66] M.J. Foral, S.H. Langer, Charactirization of sulfur layers from reduced sulfur dioxide on porous platinum black/Teflon electrodes, J. Electroanal. Chem. 246 (1988) 193.

[67] K.E. Swider, D.R. Rolison, The chemical state of sulfur in carbon-supported fuel-cell electrodes, J. Electrochem. Soc. 143 (1996) 813.

[68] D. Imamura, Effect of potential on sulfur-poisoning of Pt/C catalyst, ECS Trans 16 (2008) 807.

[69] J.A. O'Brien, J.T. Hinkley, S.W. Donne, The electrochemical oxidation of aqueous sulfur dioxide. I. Experimental parameter influences on electrode behavior, J. Electrochem. Soc. 157 (2010) F9111.

[70] I.R. Moraes, M. Weber, F.C. Nart, On the sytucture of adsorbed sulfur dioxide at the platinum electrode, Electrochim. Acta 42 (1997) 617.

[71] C. Quijada, A. Rodes, J.L. Vázquez, J.M. Pérez, A. Aldaz, Electrochemical behavior of aqueous SO_2 at Pt electrodes in acidic medium. A voltammetric and in situ FTIR study. Part II. Promoted oxidation of sulphur dioxide. Reduction of sulphur dioxide, J. Electroanal. Chem. 398 (1995) 105.

[72] Y.-E. Sung, W. Chrzanowski, A. Zolfaghari, G. Jerkiewicz, A. Wieckowski, Structure of chemisorbed sulfur on Pt (111) electrode, J. Am. Chem. Soc. 119 (1997) 194.

[73] Y.-M. Sun, D. Sloan, D.J. Alberas, M. Kovar, Z.-J. Sun, J.M. White, SO_2 adsorption on Pt (111): HREELS, XPS and UPS study, Surf. Sci. 319 (1994) 34.

[74] St Astegger, E. Bechtold, Adsorption of sulfur dioxide and the interaction of coadsorbed oxygen and sulfur on Pt (111), Surf. Sci. 122 (1982) 491.

[75] X. Lin, K.C. Hass, W.F. Schneider, B.L. Trout, Chemistry of sulfur oxides on transition metals I: configurations, energetics, orbital analyses and surface coverage effects of SO_2 on Pt (111), J. Phys. Chem. B 106 (2002) 12575.

[76] Q. Mao, U. Krewer, Total harmonic distortion analysis of oxygen reduction reaction in proton exchange membrane fuel cells, Electrochim. Acta 103 (2013) 188.